Geochimica et Cosmochimica Acta 420 (2026) 30–42

Contents lists available at ScienceDirect

Geochimica et Cosmochimica Acta

journal homepage: www.elsevier.com/locate/gca

Ferrous iron input retards denitrification and drives N_2O accumulation across salinity gradients

Jianrong Huang [a,b], Jingjing Zhao [a], Sayed Dildar Hussain [a], Mingxian Han [a], Jian Yang [a], Qing Liu [a], Andreas Kappler [c,d], Hongchen Jiang [a,b,*]

[a] School of Life Sciences, Henan University, Kaifeng 475004, China
[b] Qinghai Provincial Key Laboratory of Geology and Environment of Salt Lakes, Qinghai Institute of Salt Lakes, Chinese Academy of Sciences, Xining 810008, China
[c] Geomicrobiology, Department of Geoscience, University of Tuebingen, Tuebingen 72047, Germany
[d] Cluster of Excellence, EXC 2124, Controlling Microbes to Fight Infection, Tuebingen 72047, Germany

ARTICLE INFO

Associate editor: Caroline L. Peacock

Keywords:
Denitrification
Ferrous iron
Salinity gradients
Nitrous oxide
Microbial community

ABSTRACT

The interplay between ferrous iron (Fe(II)) and salinity in regulating nitrate reduction pathways and nitrous oxide (N_2O) emissions in lacustrine sediments remains a critical knowledge gap. This study investigated their coupled effects using sediments from Qinghai-Tibetan Plateau lakes spanning a salinity gradient (0.70–151.24 g/L), with treatments including 4 mM nitrate and 5 mM acetate (NrAc), nitrate and 5 mM Fe(II) (NrFe), and nitrate with both Fe(II) and acetate (NrFeAc). Through anoxic enrichments amended with nitrate, acetate, and/or Fe(II), the results showed that while salinity alone constrained denitrification rates, Fe(II) input (NrFe and NrFeAc) consistently retarded nitrate reduction (<13% removal in 20 days) and triggered incomplete denitrification, resulting in sustained accumulation of nitrite (~1–4 μM) and N_2O (20–60 μM). This was concurrent with Fe(II) oxidation and the formation of poorly crystalline iron minerals that extensively encrusted microbial cells. Without Fe(II) amendment (NrAc), denitrification was highly efficient (>95% nitrate removal in 72 h) with minimal accumulation of nitrite or N_2O. Microbial community analysis revealed salinity as the primary factor, selecting for halotolerant genera (e.g., *Halomonas* and *Marinobacter*) at high salinity, while Fe(II) input further increased overall species richness but reduced the predicted abundance of key denitrification genes, indicating pathway incompletion. These findings indicate that Fe(II) overrides salinity constraints to promote incomplete denitrification and N_2O production, with significant implications for nitrogen cycling in saline lakes.

1. Introduction

Denitrification, the microbial reduction of nitrate (NO_3^-) to gaseous end products such as nitrous oxide (N_2O) and dinitrogen (N_2), is a critical process in aquatic ecosystems that mitigates eutrophication and nitrogen pollution by removing reactive nitrogen species (Seitzinger et al., 2006; Burgin and Hamilton, 2007; Qi and Liu, 2023). However, incomplete denitrification can result in the accumulation of N_2O, a potent greenhouse gas with a global warming potential approximately 300 times that of CO_2, contributing significantly to climate change and ozone depletion (Ravishankara et al., 2009; Thakur and Medhi, 2019; Sun et al., 2025). The efficiency and completeness of denitrification are highly sensitive to environmental factors, including redox conditions, substrate availability, and microbial community dynamics (Zumft and Körner, 1997; Zhang et al., 2022; Gao et al., 2025). Among these, salinity has emerged as a key regulator, imposing osmotic stress and ionic toxicity that can inhibit microbial metabolism, alter enzyme activity, and reduce electron transfer efficiency, often resulting in decreased nitrate removal rates and elevated N_2O emissions (Sun et al., 2022; Sun et al., 2023; Huang et al., 2025a; Wang et al., 2025a). Globally, saline lakes account for about 44% of the total inland lake water volume (Williams, 1996; Messager et al., 2016), highlighting their importance in nitrogen cycling and greenhouse gas fluxes (Wurtsbaugh et al., 2017; Valiente et al., 2018). Despite this, the mechanisms by which salinity regulates denitrification pathways across natural salinity gradients remain poorly understood, particularly in the context of interacting biogeochemical factors (Sun et al., 2023; Wang et al., 2025a).

Salinity gradients in lacustrine systems create distinct environmental stressors that reshape microbial communities and their metabolic

* Corresponding author at: School of Life Sciences, Henan University, Kaifeng 475004, China.
E-mail address: Jiangh@henu.edu.cn (H. Jiang).

https://doi.org/10.1016/j.gca.2026.03.028
Received 24 November 2025; Accepted 12 March 2026
Available online 15 March 2026

functions. Elevated salinity not only selects for halotolerant taxa but also modifies sediment redox potential and ionic composition, which can decouple nitrogen transformation processes (Huang et al., 2022; Sun et al., 2022; Huang et al., 2023a; Torregrosa-Crespo et al., 2023). For instance, recent studies have shown that salinity stress reduces the abundance of key denitrification genes (e.g., *nirS*, *nirK*, *nosZ*), leading to incomplete nitrate reduction and increased N_2O yields (Sun et al., 2022; Pan et al., 2023b; Wang et al., 2025a). In hypersaline environments, microbial assemblages shift toward specialists like *Halomonas* and *Marinobacter*, which possess adaptations for osmotic balance but may exhibit truncated denitrification pathways (Miao et al., 2020; Huang et al., 2025b). This salinity-induced microbial restructuring underscores the need to explore how co-occurring stressors, such as iron availability, further modulate denitrification completeness and N_2O production in saline ecosystems.

Ferrous iron (Fe(II)) is another pivotal player in anoxic sediment redox networks, participating in both abiotic and microbially mediated processes that influence nitrogen cycling (Zhao et al., 2013a; Melton et al., 2014; Zhao et al., 2015; Liu et al., 2019). Nitrate-reducing Fe(II) oxidation (NrFeOx) has been documented in diverse settings, including freshwater sediments, paddy soils, marine sediments and saline lakes, where it can compete with heterotrophic denitrification for electrons and terminal acceptors (Emmerich et al., 2012; Laufer et al., 2016; Pang et al., 2021; Grimm et al., 2024). Fe(II) oxidation often generates poorly crystalline Fe(III) minerals that encrust microbial cells, potentially obstructing substrate diffusion and enzymatic activity, thereby promoting incomplete denitrification with nitrite and N_2O accumulation (Kappler et al., 2005; Klueglein et al., 2014). However, the interplay between Fe(II) and salinity in regulating these processes constitutes a critical knowledge gap. While Fe(II) may alleviate some salinity effects by providing alternative electron donors, it could also enhance N_2O emissions through mineral precipitation and redox decoupling (Huang et al., 2023b; Grimm et al., 2024). Previous work has primarily examined Fe-N interactions in isolation, with limited attention to how salinity gradients modulate these pathways in natural sediments (Emmerich et al., 2012; Huang et al., 2022).

In order to address these gaps, we hypothesized that (i) increasing salinity would constrain denitrification efficiency and shift microbial assemblages toward halotolerant taxa, and (ii) Fe(II) input would retard nitrate reduction and promote incomplete denitrification by diverting electrons to Fe(II) oxidation and inducing mineral encrustation. This study is designed to resolve the specific mechanisms through which the interplay between ferrous iron and salinity regulates the efficiency and completeness of denitrification. The primary scientific questions we seek to address are: (1) How do Fe(II) input and salinity gradients interact to control the kinetics of nitrate reduction and the accumulation of denitrification intermediates, particularly nitrite and the potent greenhouse gas N_2O? (2) To what extent do these environmental drivers individually and collectively reshape the structure and functional potential of sedimentary microbial communities? (3) What is the role of Fe(II) oxidation products, specifically the formation of poorly crystalline iron minerals and their association with microbial cells, in modifying the physicochemical microenvironment and thereby influencing denitrification pathways?

To answer these questions, we conducted a series of anoxic enrichment experiments using sediments collected from five lakes on the Qinghai-Tibetan Plateau representing a salinity gradient. The objectives of this study were to: (i) quantify the dynamics of nitrogen species (NO_3^-, NO_2^-, N_2O) and iron speciation in response to amendments of nitrate, acetate, and Fe(II); (ii) characterize the associated shifts in bacterial community composition and diversity; (iii) predict the mechanistic interactions between salinity stress, Fe(II) availability, and the completeness of denitrification pathways; and (iv) visualize the physical interactions between microbial cells and iron minerals.

2. Materials and methods

2.1. Study sites and sediment sampling

Five lakes spanning a wide salinity gradient were selected during a sampling campaign conducted in late February 2023, including Erhai Lake, Tuosu Lake, Xiaochaidan Lake, Gasikule Lake, and Keke Lake, all located on the Qinghai-Tibetan Plateau, China (Fig. S1). The study area is characterized by a typical continental arid to semi-arid climate, with mean annual precipitation ranged from 200 to 400 mm (Qin et al., 2014). The selected lakes represent distinct salinity categories: a freshwater lake with salinity <1 g L^{-1} (Erhai Lake, EHL), two mesohaline lakes with salinities of 10–30 g L^{-1} (Tuosu Lake, TSL, and Xiaochaidan Lake, XCDL), a hypersaline lake with salinity of ~70 g L^{-1} (Gasikule Lake, GSKL), and an extreme hypersaline lake with salinity of ~130 g L^{-1} (Keke Lake, KKL) (Fig. S1). Triplicate surface sediment samples (approximately 500 g wet weight per sample, 1–5 cm depth) were collected from each lake using a stainless-steel grab sampler (XDB0201, New Landmark, China), yielding a total of 15 samples for physicochemical characterization and microcosm incubation experiments. Immediately after collection, sediments were transferred into sterile polyethylene bags, sealed (not strictly anaerobic), and transported to the laboratory on ice. Porewater for initial geochemical characterization was obtained by centrifugation immediately upon sample arrival at the laboratory. These aliquots were stored at 4°C in the dark and all dissolved parameters were analyzed within one week to minimize post-sampling alteration. For the microcosm setup, sediments were handled in an anaerobic glove box (100% N_2). Triplicate sediments from each lake were homogenized to obtain a representative composite sample (Fig. S2), which was subsequently dispensed into sterile, anoxic serum bottles and stored at 4°C until the establishment of denitrification-iron redox microcosms.

2.2. Sediment physicochemical and iron speciation analyses

Sediment porewater was obtained by centrifugation at 8,000×*g* for 10 min. The pH and salinity of the porewater were measured using a portable multiparameter water analyzer (SANXIN, Shanghai, China). Concentrations of major anions (F^-, Cl^-, NO_2^-, SO_4^{2-}, NO_3^-) and cations (Na^+, NH_4^+, K^+, Mg^{2+}, Ca^{2+}) were determined by ion chromatography (IonPac AS18, 4 × 250 mm, for anions; IonPac CS12A, 4 × 250 mm, for cations; ICS 600, Thermo Fisher Scientific, USA). Prior to total organic carbon (TOC) determination, sediment samples were acidified with 1 M HCl to remove carbonates, neutralized, oven-dried, and finely ground. TOC concentrations were measured using a multi N/C 2100S analyzer (Analytik Jena, Germany). Total phosphorus (TP) and total nitrogen (TN) contents were quantified colorimetrically following established protocols (Willis et al., 1996; Neal et al., 2000).

Sequential Fe extraction was performed to quantify distinct iron fractions with increasing crystallinity using 0.5 M and 6 M HCl, following a modified protocol (Porsch and Kappler, 2011). Extractions were conducted under strictly anoxic conditions in a glove box (100% N_2 atmosphere). For bioavailable Fe extraction, approximately 1.0 g of field-moist sediment was mixed with 50 mL of anoxic 0.5 M HCl in 120 mL serum bottles and incubated in the dark for 2 h. After gentle mixing, 1.8 mL of suspension was subsampled and centrifuged at 12,000×*g* for 15 min at room temperature. For crystalline Fe extraction, 1.0 g of sediment was treated with 50 mL of anoxic 6 M HCl, incubated at 70°C for 24 h, cooled to room temperature, and centrifuged for 15 min. Fe(II) and total Fe concentrations in both bioavailable and crystalline fractions were quantified in the supernatant using the spectrophotometric ferrozine method (Stookey, 1970). All analyses were performed in technical triplicate. Iron concentrations are reported as milligrams of Fe per gram of dry sediment, corrected for sample water content. Sediment water content was determined in triplicate using the gravimetric method. Samples were weighed initially, oven-dried at 105°C for 8 h to reach a

constant weight, and then re-weighed to determine the final dry mass.

2.3. Enrichment culture setup and treatments

All microcosm incubations were conducted under strict anoxic conditions using standard sterile techniques. Enrichment cultures were established in an anoxic glovebox by adding approximately 5 g of homogenized sediment into sterile 100 mL serum bottles, which were subsequently filled with 50 mL of anoxic medium containing (per liter): 11 g $MgCl_2{\cdot}6H_2O$, 4.09 g Na_2SO_4, 1.16 g $CaCl_2$, 0.69 g KCl, 0.2 g $NaHCO_3$, 0.1 g KBr, and 0.03 g H_3BO_3. The medium was supplemented with 1 mL each of a 7-vitamin solution, a trace element solution, and a selenite-tungstate solution (Widdel and Bak, 1992). To maintain physiologically relevant salinity and pH conditions, the culture medium for each subsequent experiment was prepared to match the salinity of the source lake from which the enrichment was derived. After autoclaving, all bottles were amended with 4 mM $NaNO_3$ as electron acceptor and 5 mM sodium acetate as electron donor (NrAc). A 10% (v/v) inoculum from these stable and strict anoxic NrAc enrichments (over three successive transfers) were subsequently used to inoculate the Fe(II)-amended treatments: NrFe (5 mM $FeCl_2{\cdot}4H_2O$) and NrFeAc (5 mM sodium acetate + 5 mM $FeCl_2{\cdot}4H_2O$) (Fig. S2). After Fe(II) addition, a whitish-gray precipitate rapidly formed in the medium, indicating abiotic Fe(II) mineral precipitation (Kappler et al., 2005). All Fe(II)-amended enrichments were successively transferred at least three times prior to experimental use to ensure stable microbial consortia. Prior to incubation, the headspace was purged with N_2 for 10 min to further exclude any possible residual oxygen. Simultaneously, abiotic control treatments were established using enrichment cultures with heat-killed cells. To obtain the killed cells, the inoculum was subjected to a water bath at 80°C for 30 min. All experiments were performed in triplicate, and all bottles were incubated statically at 28°C in the dark. Throughout the incubation, aqueous samples were periodically collected for analysis of NO_3^-, NO_2^-, Fe(II), and total Fe, while N_2O in the headspace was measured by gas chromatography.

2.4. Determination of nitrate reduction and denitrification intermediates

At designated time intervals, samples were collected from the enrichment microcosms. After gentle shaking, 0.2 mL of suspension was withdrawn with a sterile syringe for NO_2^- and NO_3^- analysis, and the headspace was replenished with helium or anoxic medium to maintain pressure. For dissolved nitrogen species analysis, liquid samples were centrifuged at 12,000×*g* for 5 min, and the supernatant was appropriately diluted with deionized water prior to measurement. Nitrate (NO_3^-) concentration was determined using the Griess method (Valiente et al., 2019): diluted samples were reacted with Griess reagent, followed by addition of VCl_3 solution, incubation at 60°C for 25 min, and absorbance measurement at 540 nm using a Shimadzu UV-1750 spectrophotometer. Nitrite (NO_2^-) was analyzed by mixing diluted samples with Griess reagent, incubating for 20 min in the dark, and measuring absorbance at 540 nm. Nitrate and nitrite concentrations were determined from a standard calibration curve. At each sampling point, only 0.3 mL of liquid was withdrawn (200 μL for nitrate/nitrite analysis and 100 μL for iron determination), resulting in a cumulative volume loss of <1% of the total incubation volume over the entire experiment. For nitrous oxide (N_2O) analysis, 1 mL of headspace gas was injected into a helium-filled vial and analyzed by gas chromatography (GC-8860) equipped with an electron capture detector. Following the final time point, microbial samples from the enrichments were collected inside an anoxic glovebox. Specifically, liquid suspensions were centrifuged to pellet cells, and the resulting biomass was stored at –80°C for subsequent community analysis.

2.5. Microbial community and functional analyses

Total genomic DNA was extracted from enrichment suspensions using the Fast DNA SPIN Kit (MP Biomedicals, Santa Ana, CA, USA). The hypervariable V4 region of the bacterial 16S rRNA gene was amplified using the universal primers 515F (5′-GTGYCAGCMGCCGCGGTAA-3′) and 806R (5′-GGACTACNVGGGTWTCTAAT-3′) (Walters et al., 2015), with the reverse primer containing a unique 12-bp barcode for sample multiplexing. Each 50 μL PCR reaction contained 100 ng of purified DNA template and was amplified in triplicate under the following thermal conditions: initial denaturation at 94°C for 3 min; 35 cycles of denaturation at 94°C for 45 s, annealing at 50°C for 60 s, and extension at 72°C for 90 s; followed by a final extension at 72°C for 10 min. Amplicons (~400 bp) were pooled and purified using a DNA Gel Extraction Kit (Axygen, USA), and paired-end sequencing (2 × 250 bp) was performed on an Illumina HiSeq 2500 platform. Raw sequences were processed in QIIME2 (v2023.2) (Bolyen et al., 2019). After demultiplexing and quality filtering, reads were denoised and clustered into amplicon sequence variants (ASVs) using DADA2. Taxonomic assignment was performed against the SILVA 138 database (Quast et al., 2012). Sequences classified as chloroplasts, mitochondria, or unassigned were removed, and all samples were rarefied to 66,596 reads to standardize sequencing depth.

Alpha diversity (observed ASVs and Shannon index) and beta diversity (Bray-Curtis dissimilarity) were calculated using the "vegan" package in R (v4.5.1). Principal coordinate analysis (PCoA) was performed based on Bray-Curtis dissimilarity to visualize differences in microbial community composition across different lakes and enrichment treatments, using the "microeco" package (Liu et al., 2021). The significance of observed community differences was further assessed using PERMANOVA (Adonis) with 999 permutations. Distance-based redundancy analysis (dbRDA) with variance partitioning quantified the explanatory contributions of environmental factors Fe(II), salinity, and acetate on microbial community variation (Lai et al., 2022). Differential ASV abundance between treatments was assessed using DESeq2, and results were visualized as volcano plots with "ggplot2" package. Functional potential of denitrification pathways was predicted using PICRUSt2 in conjunction with the DiTing database for improved enzyme annotation on the Wekemo Bioincloud interactive platform (Gao et al., 2024). The analysis focused on key functional genes encoding catalytic subunits of enzymes involved in the sequential reduction process: nitrate reduction (*narG/narH/narI/napA/napB*), nitrite reduction (*nirS/nirK*), nitric oxide reduction (*norB/norC*), and nitrous oxide (*nosZ*) reduction (Xue et al., 2021). Gene abundance was normalized across all samples to enable comparative analysis of relative pathway contributions. The resulting normalized data were visualized using Sankey diagrams to illustrate the flow and proportional changes of predicted denitrification processes across different salinity levels and experimental treatments.

2.6. Mineral characterization and scanning electron microscopy

Mineral precipitates formed during Fe(II) oxidation were characterized using X-ray diffraction (XRD) and scanning electron microscopy (SEM). After 10 days of incubation, suspended solids from NrFe/NrFeAc enrichment cultures were collected by centrifugation (12,000 × *g*, 10 min) and air-dried under anoxic conditions (100% N_2 atmosphere). XRD analysis was performed using a TD-3500 diffractometer (Cu-Kα radiation, 200 kV, 45 mA) over a 2θ range of 10–90° with a step size of 0.02° and a counting time of 0.5 s per step. Diffractograms were processed using JADE 6.0 software.

Elemental composition and cell-mineral associations were analyzed using scanning electron microscopy with energy-dispersive X-ray spectroscopy (SEM-EDS). Following the Fe(II) oxidation process, liquid samples were aseptically collected from serum bottles in an anoxic glovebox and centrifuged to obtain solid precipitates. The pellets were fixed with 2.5% glutaraldehyde at 4°C for 12 h. Fixed samples were

washed three times with 0.1 M PBS buffer (15 min per wash) and dehydrated through a graded ethanol series (50, 60, 70, 80, 90, 100, and 100% with anhydrous sodium sulfate), followed by amyl acetate replacement (ethanol:amyl acetate ratios of 2:1, 1:1, and pure amyl acetate), with 15 min per step. Samples were then air-dried, coated with platinum, and imaged using a Hitachi SU8010 SEM operated at 3.0 kV with a working distance of 11.2–12.7 mm. Elemental composition of mineral coatings was determined in situ by EDS, enabling direct characterization of iron mineral encrustation on cell surfaces.

3. Results

3.1. Sediment physicochemical characteristics and iron speciation across a salinity gradient

The lakes exhibited a distinct salinity gradient, from freshwater conditions in Erhai Lake (0.7–0.84 g L^{-1}) to hypersaline environments in Keke Salt Lake (128.18–151.24 g L^{-1}) (Fig. S3). All sediments were consistently alkaline, with pH values ranging between 8.27 and 8.94, though pH did not vary systematically with salinity. In contrast, nutrient and organic matter content displayed pronounced negative correlations with increasing salinity. Total nitrogen (TN) decreased from 489.06–678.46 μg/g in EHL to 177.68–379.28 μg/g in higher-salinity lakes, while total phosphorus (TP) declined from 480.3–534.28 μg/g to 371.73–477.74 μg/g. Similarly, total organic carbon (TOC) was highest in EHL (14.12–14.86 mg/g) and lowest in KKL (3.86–13.19 mg/g). The water content of the sediments (determined by weight loss after heating the sediments) ranged from 27.44 to 69.93%.

Both bioavailable and crystalline iron were detected in sediments from all lakes across the salinity gradient (Fig. 1). Crystalline iron consistently exceeded bioavailable fractions, indicating active iron mineralization. Specifically, bioavailable Fe(II) ranged from 1.56 to 7.17 mg/g dry sediment, while total bioavailable Fe varied between 2.47 and 7.24 mg/g dry sediment (Fig. 1A). For crystalline iron, Fe(II) spanned 9.87–16.27 mg/g dry sediment, and total crystalline Fe ranged from 14.74 to 22.58 mg/g dry sediment (Fig. 1B).

3.2. Effects of salinity and Fe(II) input on nitrate reduction

Across the salinity gradient, NrAc enrichment cultures exhibited a clear salinity-dependent retardation of denitrification (Fig. 2A). Specifically, the rate of nitrate depletion decreased progressively with increasing salinity, while the transient accumulation of nitrite and subsequent N_2O production also displayed slower kinetics in higher salinity enrichment cultures. Together, these observations indicate that escalating salinity constrains the efficiency of acetate driven denitrification. In contrast, both NrFe and NrFeAc enrichment cultures showed markedly retarded nitrate reduction across all salinity levels compared to NrAc (Fig. 2B and 2C). More critically, the addition of Fe(II) induced incomplete denitrification, as demonstrated by the sustained accumulation of nitrite and N_2O over time, rather than their complete reduction to N_2. Simultaneously, the decline in the Fe(II) to total Fe ratio in NrFe and NrFeAc treatments confirmed the oxidation of Fe(II) coupled with microbial nitrate reduction, and potentially abiotic processes such as chemodenitrification (Fe(II)-driven nitrite reduction) and abiotic Fe(II) oxidation by nitrate/nitrite. Nevertheless, this iron mediated electron transfer failed to support the complete denitrification pathway, resulting in the accumulation of intermediate products. Time-course analysis of control enrichment cultures confirmed the absence of significant nitrogen or iron redox transformation under all experimental conditions (Fig. S4). Specifically, abiotic controls containing heat-killed cells exhibited no Fe(II) oxidation or nitrate reduction. Neither nitrite accumulation nor N_2O production was detected in any of these controls.

3.3. Denitrification efficiency under salinity and Fe(II) influence

Analysis of nitrate removal efficiency, nitrite production, and nitrous oxide production across enrichment cultures from lakes spanning a salinity gradient revealed that Fe(II) input consistently retarded nitrate reduction and led to incomplete denitrification, irrespective of salinity. In the NrAc treatment, nitrate removal exceeded 95% in 72 h across all salinities, with negligible accumulation of nitrite and N_2O, indicating efficient and complete denitrification. In contrast, both the NrFe and NrFeAc treatments exhibited severely limited nitrate removal (<13% in

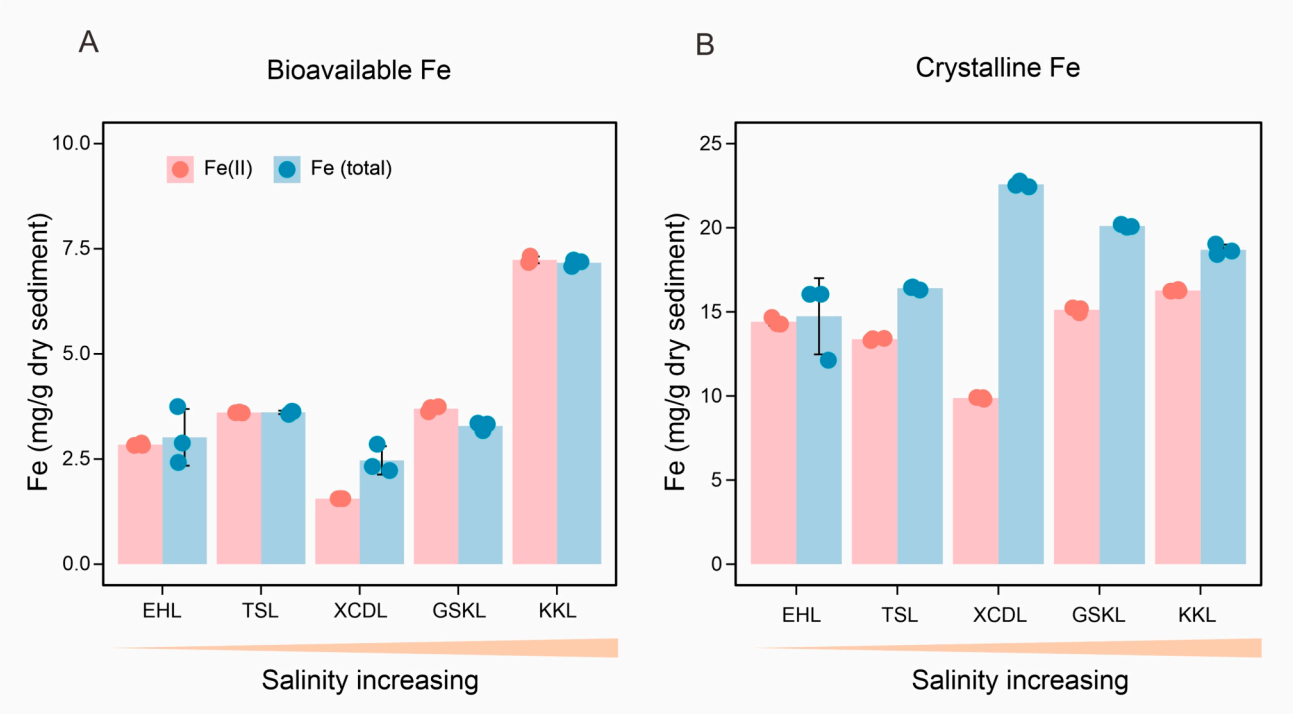

Fig. 1. Concentrations of bioavailable Fe (A) and crystalline Fe (B) in sediments from five lakes along salinity gradients.

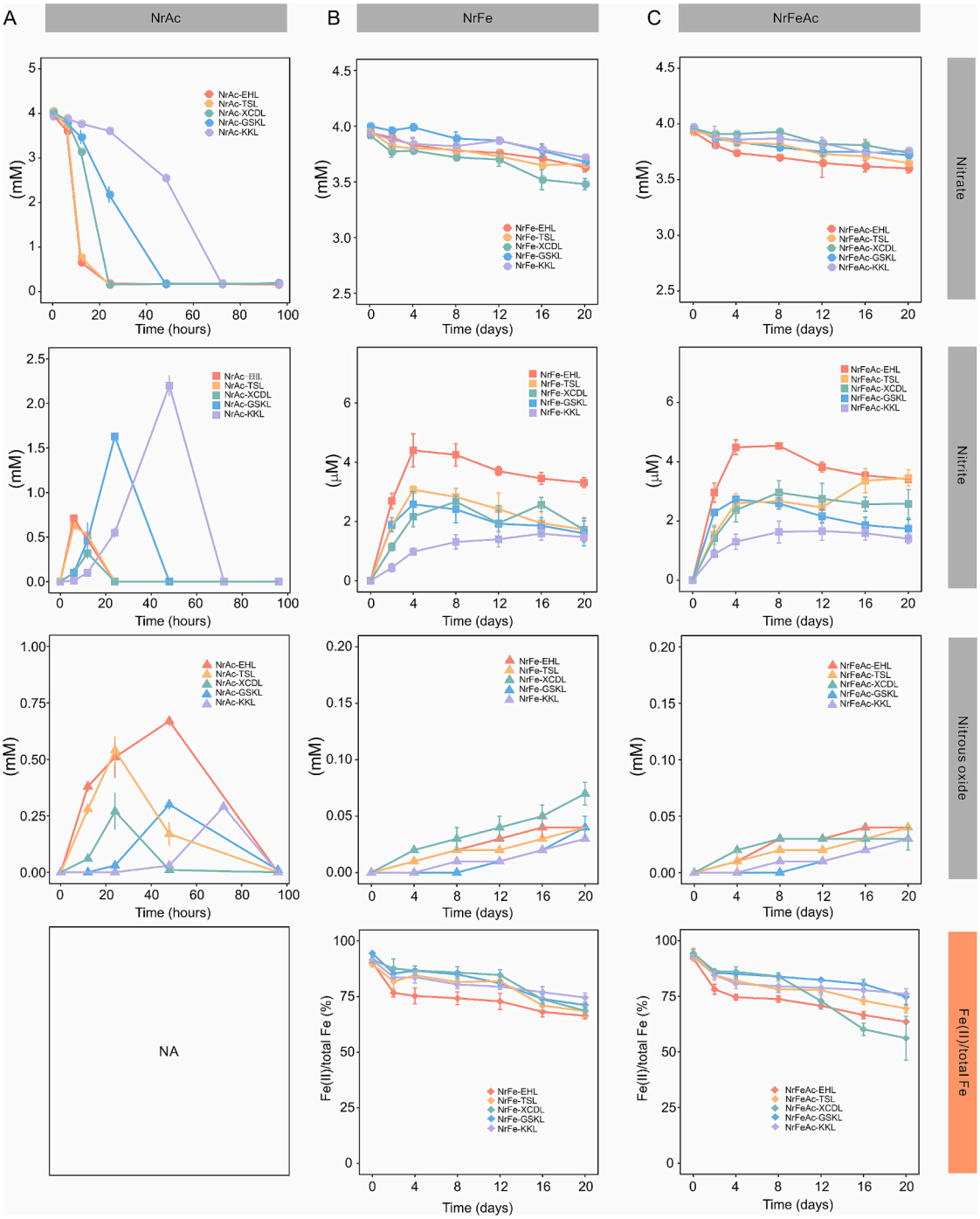

Fig. 2. Time-course variations of nitrate, nitrite, nitrous oxide and Fe(II)/total Fe ratio, concentrations in the enrichment cultures under NrAc (A), NrFe (B), and NrFeAc (C) conditions along salinity gradients. Note that the x-axis units differ across treatments to accommodate varying reaction kinetics: time is expressed in hours for NrFe and in days for NrAc and NrFeAc. The initial Fe(II) concentration in the NrFe and NrFeAc treatments was 5.0 mM, resulting in a molar Fe/N ratio of 5:4 relative to the supplied nitrate (4.0 mM).

20 days) alongside sustained accumulation of nitrite (~1–4 μM) and N_2O (20–60 μM) (Fig. 3A), demonstrating Fe(II)-induced disruption of the denitrification pathway. Furthermore, linear regression analyses illustrated a strong negative correlation between average nitrate reduction rates and salinity in the NrAc treatment ($R^2 = 0.89$, $p < 0.001$), highlighting significant salinity inhibition. This inhibitory effect was attenuated in Fe(II)-amended systems (NrFe: $R^2 = 0.27$, $p < 0.05$; NrFeAc: $R^2 = 0.45$, $p < 0.01$) (Fig. 3B), suggesting that Fe(II) input not only impairs denitrification completeness but also alters its responsiveness to salinity stress.

3.4. Microbial community diversity and taxonomic differentiation among different treatments

Analysis of bacterial community structure revealed that both Fe(II) input and salinity significantly influenced diversity and composition in the enrichment cultures. Alpha diversity index showed that species richness was significantly ($p < 0.001$) lower in the NrAc treatment compared to the NrFe and NrFeAc treatments (Fig. 4A), which exhibited markedly higher richness, though the Shannon index indicated no significant differences in evenness across treatments (Fig. 4B). Genus-level

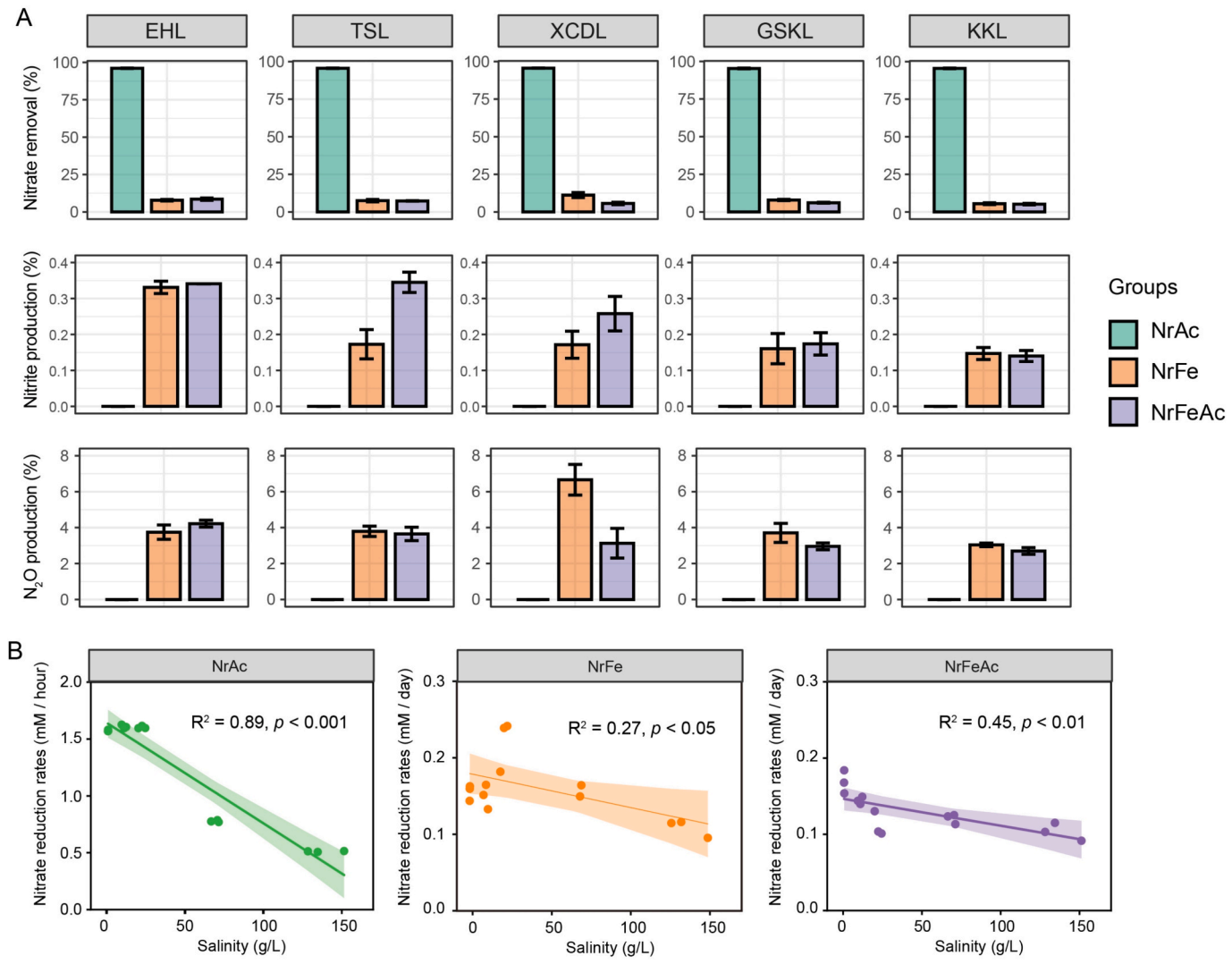

Fig. 3. (A) Nitrate removal efficiency, nitrite production, nitrous oxide production in enrichment cultures along salinity gradients, where different bars for each treatment represent data at two distinct time points (100 h vs. 20 days); (B) linear correlations between mean nitrate reduction rates and salinity.

composition further demonstrated clear shifts linked to both Fe(II) input and salinity: low-salinity enrichments were dominated by taxa such as *Pseudomonas* and *Thauera*, whereas high-salinity conditions selected for halotolerant genera including *Halomonas* and *Marinobacter* in NrAc, and *Halanaerobium, Halomonas* and *Marinobacter* in Fe(II)-amended systems (Fig. 4C). Prior to enrichment, sediments displayed distinct genus-level community compositions along the salinity gradient (Fig. S5), dominated by unclassified and uncultured taxa, with *Sulfurovum*, *Sulfurimonas*, *Thiobacillus*, and *Halanaerobium* as major classified genera. These baseline communities differed substantially from those observed after experimental enrichment. PCoA based on Bray-Curtis dissimilarity confirmed that bacterial communities clustered strongly along a salinity gradient, explaining a substantial portion of the variance ($R^2 = 0.62$, $p < 0.001$) (Fig. 4D). Distance-based redundancy analysis (dbRDA) further identified salinity, Fe(II), and acetate as significant explanatory variables structuring community composition (Fig. 4E). Together, these results indicate that Fe(II) input enhances species richness, while salinity emerges as a key environmental filter, with both factors collectively restructuring microbial communities in a manner consistent with observed differences in denitrification function.

Volcano plot analysis revealed significant, salinity-modulated restructuring of microbial communities at the ASV level in response to different treatments. Relative to the acetate-only (NrAc) treatment, both NrFe and NrFeAc enrichments exhibited substantial ASV enrichment ($Log_2FoldChange > 2$) and depletion ($Log_2FoldChange < -2$) across the five lakes (Fig. 5). Specifically, in comparison to the NrAc treatment, ASVs classified as *Pseudomonas*, *Acinetobacter*, *Desulfotignum*, *Sphingopyxis* and *Marinobacter* were notably enriched in the NrFe and NrFeAc treatments, whereas ASVs affiliated with *Marinobacter*, *Halomonas* and *Lentimicrobium* were depleted (Fig. 5). Pairwise comparisons further indicated that the most pronounced community shift occurred between NrAc and NrFe/NrFeAc, highlighting a major transition in metabolic guilds driven by Fe(II) availability. The contrast between NrFe and NrFeAc revealed fewer differential ASVs, suggesting functional overlap when Fe(II) is present.

3.5. Predicted denitrification pathways

The denitrification process involves a sequential reduction from nitrate to nitrite, nitric oxide, nitrous oxide, and ultimately to dinitrogen gas, represented by four key pathway modules. Predicted pathway analysis indicated that denitrification potential was already present in the original sediments prior to enrichment, although the relative contributions of individual pathway steps were markedly lower than those in the enrichment treatments (Fig. S6). Following enrichment, the relative contributions of these pathways differed significantly among

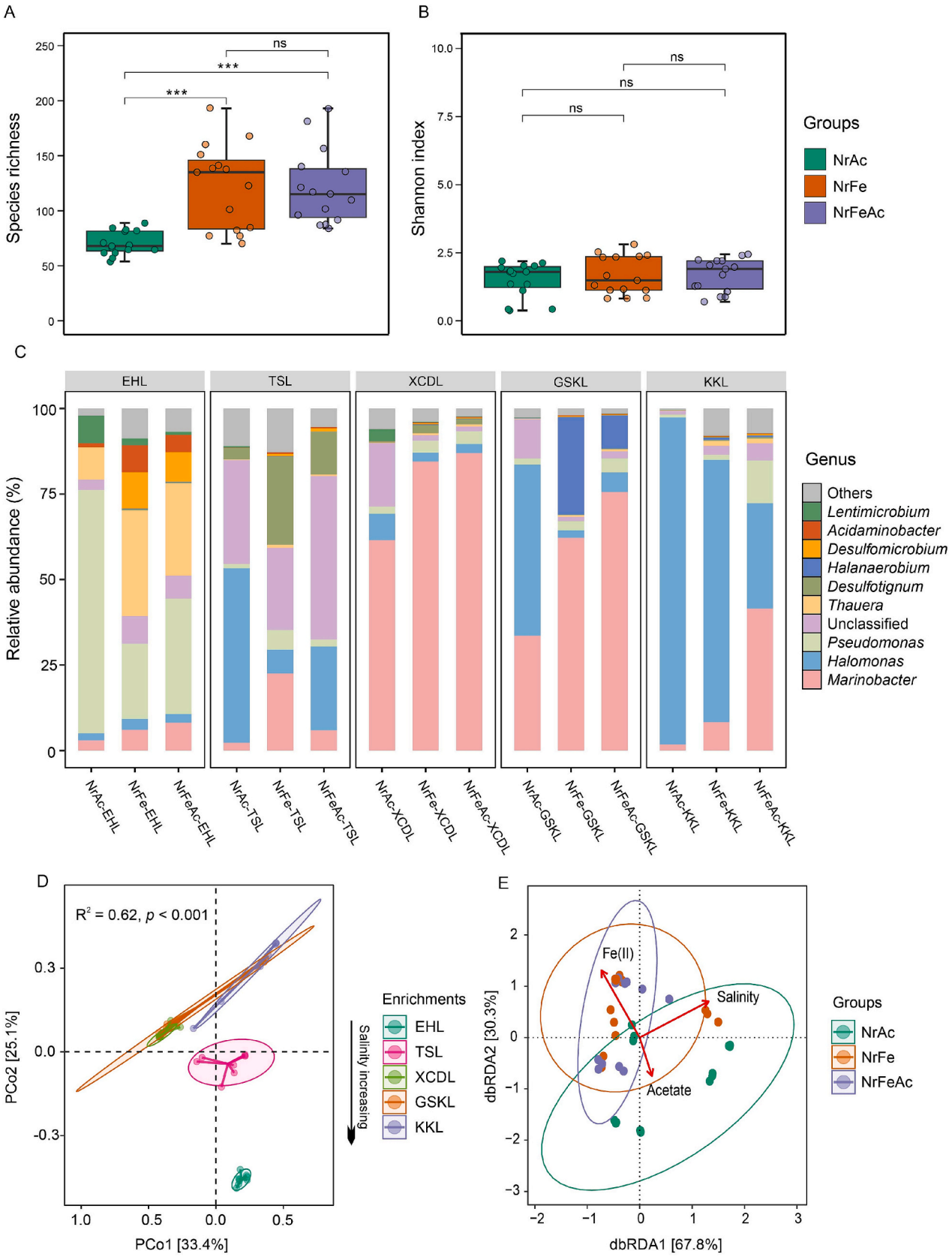

Fig. 4. Changes in microbial community diversity, composition, and structure in enrichment cultures along salinity gradients. Panels show alpha diversity indices (species richness, A; Shannon index, B), genus-level community composition (C), principal coordinate analysis (PCoA) of community structure across salinity levels (D), and distance-based redundancy analysis (dbRDA) illustrating the relative influences of Fe(II), salinity, and acetate on microbial community variation (E).

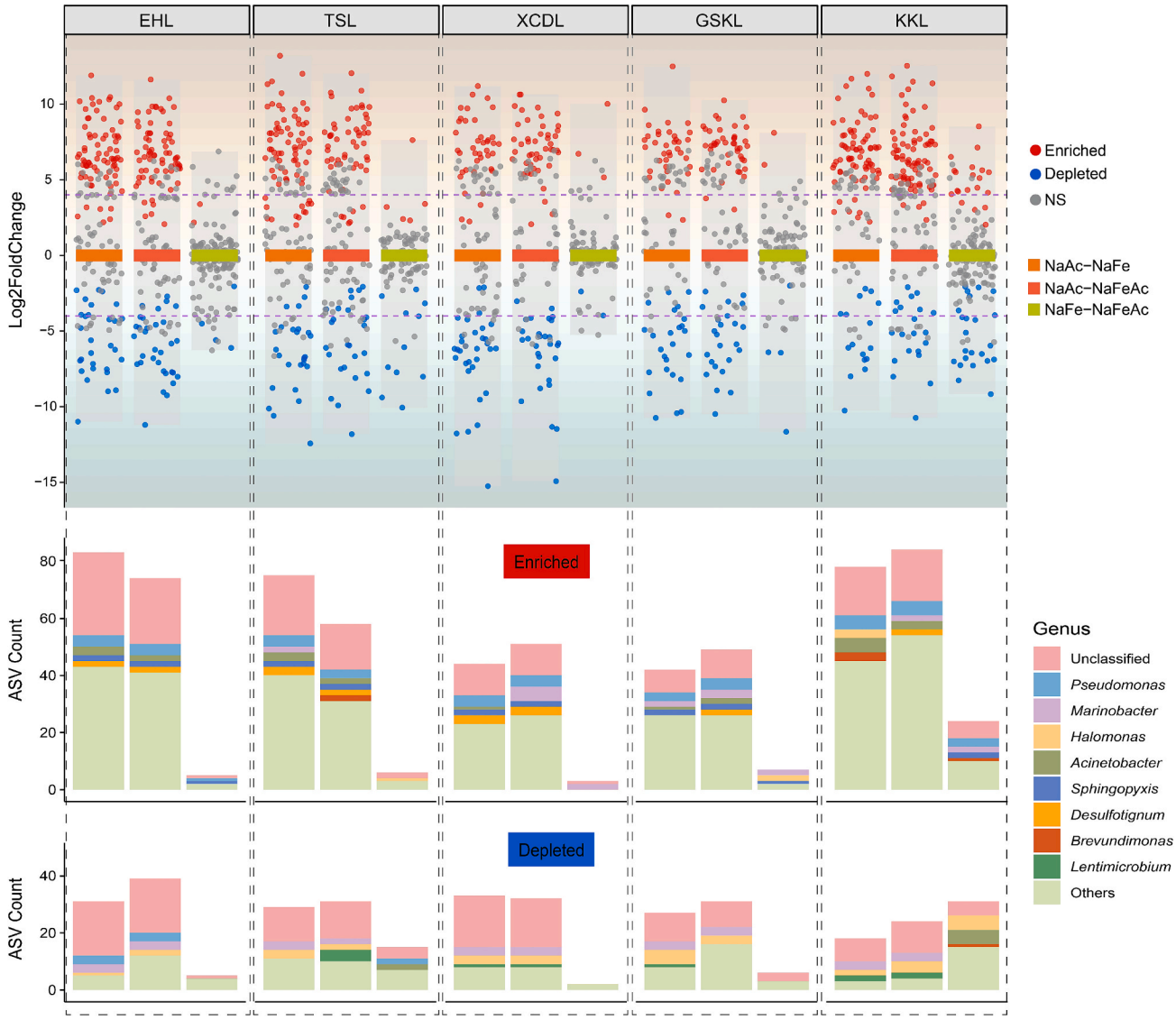

Fig. 5. Volcano plots and taxonomic composition illustrating differential Amplicon Sequence Variants (ASVs) among NrAc, NrFe, and NrFeAc treatments across enrichments from five lakes (EHL, TSL, XCDL, GSKL, KKL) along salinity gradients.

treatments (Fig. S6). In the NrAc group, the complete denitrification process was dominant, with strong activities observed in the reduction of nitrate to nitrite, nitrite to nitric oxide, nitric oxide to nitrous oxide, and nitrous oxide to nitrogen. In contrast, both NrFe and NrFeAc treatments exhibited lower relative contributions across all stages of the denitrification pathway, suggesting that the presence of ferrous iron may constrain complete denitrification activity. Across the six studied lakes, the predicted denitrification pathways displayed a clear distribution trend along the salinity gradient. High-salinity lakes such as KKL and GSKL exhibited lower relative contributions to denitrification, whereas low-salinity lakes such as EHL showed strong activities.

3.6. *Microscopic evidence of Fe–microbe interactions*

SEM analysis revealed distinct differences in microbial cell morphology and iron mineral associations across the experimental treatments. In the NrAc enrichment cultures, microbial cells displayed well-defined, unencumbered morphologies such as rod-shaped and coccobacillary forms, existing either individually or in loose aggregates (Fig. 6A). Moreover, with increasing salinity, cells were observed to preferentially attach to salt crystals. In contrast, both NrFe and NrFeAc treatments exhibited extensive cell-mineral interactions, with cells frequently encrusted by poorly crystalline, granular iron precipitates and embedded within iron-rich matrices (Fig. 6B and C). The widespread occurrence of iron mineral encrustation across Fe(II)-amended systems corresponds with Fe(II) oxidation processes and aligns with the observed retardation of nitrate reduction and incomplete denitrification, suggesting that iron mineral formation physically and chemically modifies the microbial microenvironment, thereby influencing metabolic function.

No distinct reflections corresponding to crystalline iron(III) (oxyhydr)oxides (e.g., goethite, magnetite) were detected in NrFe and NrFeAc treatments (Fig. S7), implying that iron minerals formed in these cultures are either poorly crystalline (falling below XRD's detection limit for crystallinity) or present at concentrations too low (<5–10%) to be resolved against the halite background. SEM-EDS analysis of precipitates from Fe(II)-amended enrichment cultures revealed regularly shaped mineral aggregates with distinct prismatic, cubic, and tabular morphologies, indicating ordered crystallization under chemical/microbial mediation. Energy-dispersive X-ray spectroscopy consistently detected iron in these mineral phases, alongside dominant elements including sodium, chlorine, and oxygen, as well as trace constituents

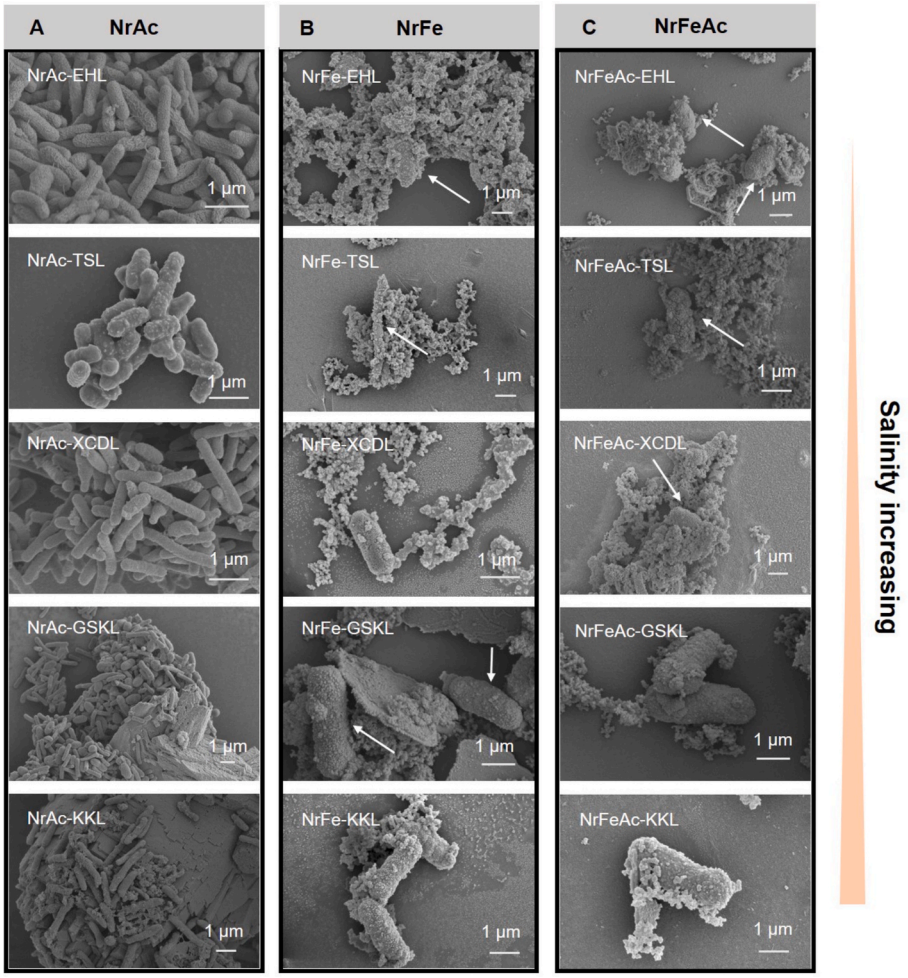

Fig. 6. Scanning electron microscopy (SEM) micrographs depicting microbial cell morphology and iron mineral associations in enrichment cultures under NrAc (A), NrFe (B), and NrFeAc (C) conditions across a salinity gradient.

such as calcium (Fig.S8), confirming the incorporation of Fe into the mineral matrix derived from Fe(II) oxidation.

4. Discussion

4.1. Coupled influences of salinity and ferrous iron on denitrification kinetics

Our results demonstrate that both salinity and Fe(II) availability exert strong and interactive controls on nitrate reduction in lacustrine sediments. The observed progressive inhibition of denitrification with increasing salinity in the acetate-only treatments (NrAc) is consistent with a growing body of literature documenting the detrimental effects of osmotic stress and ionic toxicity on metabolism and electron transfer efficiency in denitrifying microorganisms (Zhao et al., 2013b; Yang et al., 2022; Sun et al., 2023; Xia et al., 2025). The significant negative correlation between average nitrate reduction rates and salinity (R^2 = 0.89, $p < 0.001$) in NrAc systems (Fig. 3B) underscores salinity as a primary variable constraining heterotrophic denitrification efficiency. This inhibition likely stems from the combined effects of impaired enzyme conformation and activity, as well as disrupted substrate transport across cell membranes under high osmotic pressure (Zhao et al., 2013b; Gao et al., 2025). For instance, a recent study demonstrated that elevated salinity and alkalinity significantly decreased denitrification genes (*nirK*, *nirS*, and *nosZ*), leading to a 44.57–63.24% decline in denitrification activity along a salt–alkali gradient ranging from 0.5 to 8‰ (Pan et al., 2023b). Our findings extend this understanding by demonstrating that this salinity-induced retardation occurs across a remarkably wide natural gradient (0.70–151.24 g/L), with consequential delays in the short duration and turnover of denitrification intermediates like nitrite and N_2O (Fig. 2A).

Fe(II) input acts as a powerful disruptor of denitrification completeness, irrespective of the salinity level. The stark contrast between the NrAc treatment (>95% nitrate removal in 72 h with minimal intermediate accumulation) and the Fe(II)-amended systems (NrFe and NrFeAc, with <13% nitrate removal in 20 days and sustained accumulation of nitrite and N_2O) demonstrates that Fe(II) introduction fundamentally alters the biogeochemical trajectory of nitrate reduction (Fig. 2 and Fig. 3A). The concurrent decline in the Fe(II)/Fe(total) ratio in these treatments confirms active Fe(II) oxidation, implicating it in the observed nitrate reduction. However, this process failed to support a complete denitrification cascade, instead stalling at intermediate products. This aligns with the concept of nitrate-reducing Fe(II) oxidation, which often terminates at nitrite or N_2O due to thermodynamic and enzymatic constraints (Zhang et al., 2019; Jakus et al., 2021; Huang et al., 2023b; Grimm et al., 2024). The attenuation of the correlation strength between nitrate reduction rates and salinity in Fe(II)-amended treatments indicates that the dominant control mechanism shifts from osmotic stress to the microscale redox heterogeneity induced by Fe(II). This shift is mediated primarily through Fe(III) mineral precipitation, which generates new redox niches and physical barriers at the cell-mineral interface.

The retardation and incompleteness of denitrification in Fe(II)-amended treatments likely arise from a combination of biochemical

and physicochemical constraints. Biochemically, Fe(II) competes with organic carbon (when present) as an alternative electron donor. This competition appears to divert electron flow away from the energetically less favorable later steps of denitrification, particularly the reduction of N_2O to N_2 catalyzed by NosZ (Li et al., 2022; Wang et al., 2025b). This mode of regulation is expected to be most pronounced at lower Fe(II) inputs, where denitrification remains predominantly enzyme-mediated but becomes functionally incomplete due to altered electron partitioning. The functional gene prediction analysis (Fig. S6), which showed lower relative contributions of all denitrification pathway modules in Fe (II)-amended treatments, supports this biochemical decoupling. In contrast, at higher Fe(II) concentrations, physicochemical constraints likely become increasingly important. Rapid Fe(II) oxidation promotes the formation of poorly crystalline Fe(III) minerals that extensively encrust microbial cells, as observed by SEM (Fig. 6), generating diffusion-limited microenvironments and pronounced redox heterogeneity. These mineral coatings can impede the mass transfer of substrates (NO_3^-) and gaseous intermediates (N_2O), thereby hindering enzymatic turnover independently of electron availability (Kappler et al., 2005; Klueglein et al., 2014; Zhao et al., 2017; Huang et al., 2022; Hu et al., 2023). The absence of detectable crystalline Fe(III) phases in our XRD analysis (Fig. S7) further indicates the dominance of poorly ordered, reactive minerals that are particularly effective at coating cell surfaces and aggregating cells into matrices, further restricting metabolic activity. Collectively, these mechanisms illustrate a metabolic transition from highly efficient, complete heterotrophic denitrification towards to low efficient, and incomplete, Fe-N coupling regime driven by Fe(II) oxidation.

The nitrate, acetate, and Fe(II) concentrations used in the enrichment experiments exceed porewater levels commonly reported for lake sediments, including those from the Qinghai-Tibetan Plateau. These elevated concentrations were not intended to quantitatively reproduce in situ conditions, but to establish a controlled, process-based end-member system that allows mechanistic resolution of Fe-salinity interactions, electron partitioning, and mineral–microbe coupling across a broad salinity gradient. Extrapolation to natural sediments therefore involves uncertainty in absolute N_2O fluxes due to lower substrate availability, redox variability, and spatial heterogeneity. Nevertheless, the mechanisms identified here are expected to be relevant wherever Fe (II) becomes locally concentrated, such as in redox transition zones or during episodic Fe mobilization. Consequently, while absolute fluxes cannot be directly inferred, the experimental results highlight mechanistic pathways through which Fe-N coupling can shift sediments from effective nitrogen removal toward sustained N_2O production, with important implications for predicting greenhouse gas emissions from salinizing inland waters.

4.2. Salinity and Fe(II) as structuring forces on microbial community assembly

Salinity emerged as a dominant environmental filter, while Fe(II) input created additional ecological niches that reshaped microbial community structure. Increasing salinity consistently selected for halotolerant taxa such as *Halomonas* and *Marinobacter* at high salinity, whereas communities at lower salinity were dominated by non-halophilic denitrifiers including *Pseudomonas* and *Thauera* (Fig. 4C). This finding is consistent with prior studies in hypersaline denitrifying systems. For example, our prior work reported similar dominance of *Halomonas* in hypersaline heterotrophic denitrifying processes (Huang et al., 2022). Similarly, a previous work demonstrated that elevated salinity substantially reshapes denitrifying microbial communities in biofilm reactors, where halophilic genera such as *Halomonas* and *Marinobacter* cooperatively maintain denitrification activity under hypersaline stress (Huang et al., 2025b). These taxa possess sophisticated adaptations for osmotic balance, such as the accumulation of compatible solutes, allowing them to maintain metabolic activity under conditions that inhibit non-halotolerant organisms (Torregrosa-Crespo et al., 2023).

Fe(II) addition emerged as a significant secondary factor that enhanced overall species richness (Fig. 4A) and promoted the coexistence of taxa associated with Fe-related metabolisms. Analysis of relative abundance data indicated an enrichment of genera such as *Pseudomonas*, *Acinetobacter*, *Desulfotignum*, *Sphingopyxis* and *Marinobacter* in Fe(II)-amended treatments aligns with their known capabilities for Fe-associated metabolism (Handley and Lloyd, 2013; Su et al., 2015). However, these shifts coincided with decreased denitrification completeness, implying that Fe(II) fosters functional redundancy among Fe-N cycling taxa that favor energetically efficient but truncated nitrate reduction (Huang et al., 2023b). Consequently, Fe(II) and salinity jointly restructure microbial communities (Jiang et al., 2021; Yang et al., 2021), stabilizing Fe-N coupling but compromising complete nitrogen removal. Crucially, as these findings are inferred from relative abundance data, further quantitative validation is required to distinguish between absolute population expansion and relative compositional turnover.

4.3. Functional decoupling between nitrate reduction and N_2O mitigation

A central and environmentally significant finding of this study is the accumulation of N_2O in Fe(II)-amended treatments. This demonstrates a critical functional decoupling between the initial step of nitrate reduction and the final, mitigating step of N_2O reduction to N_2. The accumulation of 20–60 μM N_2O in the headspace of NrFe and NrFeAc systems (Fig. 2 and 3A) highlights a previously underappreciated risk associated with Fe(II) availability in saline sediments. The suppression of *nosZ*-mediated N_2O reduction in Fe(II)-rich systems may be attributed to several mechanisms. First, Fe(II)-induced changes in redox potential and localized oxygen gradients could destabilize *nosZ* expression or enzyme activity (Liu et al., 2019). Second, the formation of Fe-bearing mineral coatings may restrict N_2O diffusion and hinder enzyme-substrate interactions (Pan et al., 2023a). Third, abiotic nitrite (NO_2^-) reduction by Fe(II), known as *chemodenitrification*, provides a non-enzymatic pathway for N_2O production (Buchwald et al., 2016; Zhao et al., 2017). Given the sustained coexistence of these reactants and the dominance of poorly crystalline Fe minerals, chemodenitrification likely represents a substantial and continuous contribution to the observed N_2O pool. In parallel, competition occurs at the level of electron allocation, with Fe(II) oxidation and heterotrophic metabolism acting as concurrent electron-donating processes that divert reducing power away from the energetically less favorable terminal step of denitrification, thereby limiting N_2O reduction to N_2 (Wang et al., 2016; Li et al., 2022). Comparable Fe-related enhancement of N_2O accumulation has been reported in a pyrite-rich limestone aquifer (Jakus et al., 2021) and enrichment culture KS (Huang et al., 2023b), supporting the interpretation that Fe(II) promotes incomplete denitrification and increases N_2O emissions under reducing conditions. Moreover, Fe(II) availability appears to weaken the dependence of denitrification on salinity, as indicated by lower R^2 values in Fe (II)-amended regressions (Fig. 3B). This shift suggests that under elevated Fe(II) concentrations, mineral-microbe interactions, particularly Fe(III) mineral precipitation on cell surfaces, rather than osmotic stress, become the dominant control on nitrate reduction (Wang et al., 2025b). The formation of Fe-bearing minerals not only constrains denitrification kinetically but also alters nitrogen turnover timescales, leading to the persistence of incomplete denitrification within sedimentary environments. These zones likely act as long-term reservoirs for reactive nitrogen intermediates and as hotspots for N_2O release to the water column and atmosphere.

The separation of nitrate reduction from its complete endpoint (N_2) suggests that in iron-rich saline lakes, even when nitrate is being actively reduced, the ecosystem may function as a net source of N_2O rather than a sink for reactive nitrogen. This finding critically addresses the knowledge gap identified in the introduction regarding the implications

of Fe-N coupling for N_2O production. The work on lake-groundwater interfaces (Wang et al., 2025b) and in paddy soils (Grimm et al., 2024) similarly point to Fe(II) as a key driver of N_2O accumulation. Our study confirms this phenomenon across a wide salinity spectrum in natural lake sediments, significantly expanding the environmental contexts where this feedback loop must be considered. The weakening of the salinity-nitrate reduction rate correlation in the presence of Fe(II) (Fig. 3B) further implies that in Fe(II)-rich environments, the primary control on N_2O emissions may shift from osmotic stress to the kinetics of Fe mineral formation and electron partitioning, a transition with major implications for predicting greenhouse gas fluxes from salinizing inland waters. It should be noted that ammonium was not systematically quantified in this study, which limits direct evaluation of ammonium-producing pathways such as DNRA or Feammox (Shu et al., 2016). Future studies incorporating ammonium measurements and isotopic tracing will be required to more comprehensively resolve the coexistence and relative importance of parallel nitrogen transformation pathways.

4.4. Conceptual model of denitrification under salinity and Fe(II) stress

Synthesizing our geochemical and microbiological findings, we propose an integrated conceptual model that describes the mechanistic transition in sedimentary denitrification driven by the interplay of salinity and Fe(II) (Fig. 7). This conceptual model incorporates the proposed concentration-dependent mechanisms, wherein electron competition is hypothesized to dominate at lower Fe(II) inputs, while physicochemical constraints via mineral encrustation become increasingly prominent at higher concentrations. Under low-salinity conditions with organic carbon as the sole electron donor (NrAc), denitrification proceeds efficiently along a well-defined pathway, facilitated by a microbial community dominated by classic denitrifiers like *Pseudomonas* and *Thauera*. Electron flow is directed efficiently through the denitrification cascade, resulting in rapid nitrate removal and complete reduction to N_2 with minimal intermediate accumulation.

As salinity increases, osmotic stress becomes the primary constraint. It inhibits microbial metabolism and electron transfer efficiency across the entire community, slowing down the kinetics of each denitrification step. While the pathway may still proceed to completion, the process is significantly retarded, leading to an extended residence time of nitrogen intermediates in the system. The community shifts towards halotolerant specialists like *Halomonas* and *Marinobacter*, which maintain activity but potentially at a lower overall rate.

The introduction of Fe(II) fundamentally rewires this system. It introduces a competing electron donor that is preferentially utilized, diverting electrons away from the later, less energetically favorable steps of denitrification, particularly the N_2O reduction catalyzed by NosZ. Concurrently, the oxidation of Fe(II) generates poorly crystalline Fe(III) minerals that extensively encrust microbial cells. This mineral precipitation creates diffusion-limited microzones that physically impede substrate and product transport, further exacerbating the biochemical decoupling. The microbial community responds by enriching for iron-cycling taxa, increasing overall richness but functionally stabilizing a state of incomplete nitrogen cycling. The system transitions from being a nitrogen-removing sink to an incomplete nitrogen trap, where nitrate reduction is initiated but stalls, leading to the sustained accumulation and potential release of nitrite and N_2O. In this conceptual model, salinity acts as a key regulator that sets the baseline rate of the denitrification process, while Fe(II) introduction selectively impairs its terminal step, thereby obstructing the mitigation of N_2O.

5. Conclusion

This study establishes that ferrous iron (Fe(II)) input acts as a critical regulator of denitrification pathways in lacustrine sediments across a natural salinity gradient (0.70–151.24 g/L), fundamentally shifting the system from efficient nitrogen removal to incomplete denitrification with sustained accumulation of nitrous oxide (N_2O). While salinity alone constrains denitrification efficiency by imposing osmotic stress on microbial metabolism, Fe(II) introduction overrides this salinity-dependent inhibition by competing for electrons, promoting nitrate-reducing Fe(II) oxidation, and inducing the formation of poorly crystalline iron minerals that encrust microbial cells, thereby creating diffusion-limited microenvironments. Microbial community patterns indicate that while salinity structures community composition by selecting for halotolerant taxa, Fe(II) availability reshapes functional outcomes by increasing community richness but reducing the effectiveness of key denitrification steps, leading to functional decoupling between nitrate reduction and N_2O mitigation. The conceptual model underscores that Fe(II) shifts the system from efficient nitrogen removal to incomplete denitrification, where salinity sets the baseline denitrification kinetics, but Fe(II) disrupts the terminal steps, enhancing N_2O

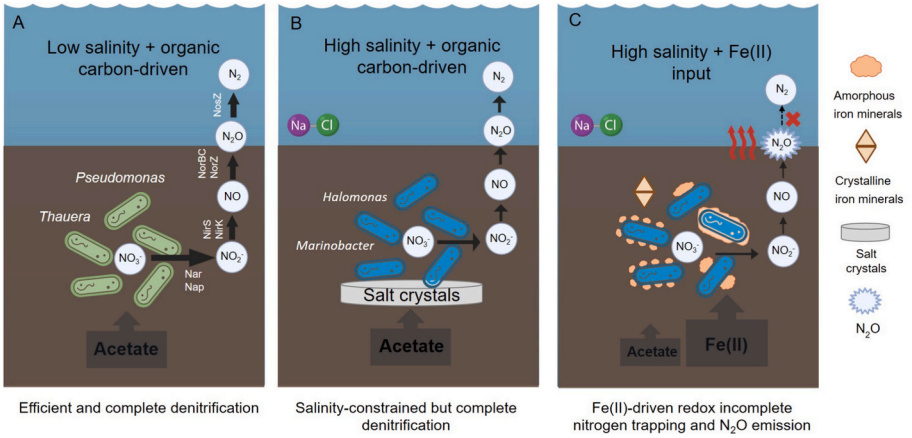

Fig. 7. Conceptual model illustrating the mechanistic regulation of sedimentary denitrification by salinity and ferrous iron (Fe(II)). Under low-salinity conditions with organic carbon as the sole electron donor, denitrification proceeds efficiently and completely to N_2, supported by canonical heterotrophic denitrifiers. Increasing salinity imposes osmotic stress that constrains microbial metabolism and electron transfer, slows denitrification kinetics, and prolongs the residence time of nitrogen intermediates, while favoring halotolerant taxa. In contrast, Fe(II) input fundamentally alters electron flow by introducing a competing electron donor, diverting electrons away from the energetically less favorable terminal step of N_2O reduction. Concurrent Fe(II) oxidation promotes the formation of poorly crystalline Fe(III) minerals that encrust microbial cells, with the relative importance of electron competition and mineral encrustation likely varying with Fe(II) availability, generating diffusion-limited microenvironments and further suppressing complete denitrification. Together, these processes shift the system from efficient nitrogen removal toward to incomplete denitrification characterized by persistent nitrite and N_2O accumulation.

emissions. These findings highlight the dual control of Fe(II) and salinity on greenhouse gas production, with implications for predicting nitrogen cycling dynamics in iron-rich saline lakes under global change.

Data availability

All sequence data were uploaded to the NCBI Sequence Read Archive database (accession number: PRJNA1353666). Sediment physicochemical characteristics, X-ray diffractograms, and iron reduction kinetic data analyzed in this study are available through Mendeley Data at: https://data.mendeley.com/datasets/zw55ybbmjn/1.

CRediT authorship contribution statement

Jianrong Huang: Funding acquisition, Data curation, Methodology, Formal analysis, Writing - original draft, Writing – review & editing. **Jingjing Zhao:** Methodology, Formal analysis, Data curation. **Sayed Dildar Hussain:** Methodology, Data curation. **Mingxian Han:** Resources, Methodology, Formal analysis. **Jian Yang:** Funding acquisition, Methodology, Software. **Qing Liu:** Methodology, Software. **Andreas Kappler:** Supervision, Writing – review & editing. **Hongchen Jiang:** Conceptualization, Supervision, Writing – review & editing.

Declaration of competing interest

The authors declare that they have no known competing financial interests or personal relationships that could have appeared to influence the work reported in this paper.

Acknowledgments

This research was funded by the National Natural Science Foundation of China (grant no. 42202338, 42272356), the China Postdoctoral Science Foundation under Grant Number 2022M722933, the Qinghai Provincial Key Laboratory of Geology and Environment of Salt Lakes (The Science and Technology Plan Project of Qinghai Province Incentive Fund, grant No. 2024-KFKT-A08.

Appendix A. Supplementary material

These materials include additional methodological details, figures, and datasets that support the main text, specifically: Diagrams illustrating the geographic distribution of sampling lakes along a salinity gradient on the Qinghai-Tibetan Plateau; A schematic workflow of the experimental design for denitrification-iron redox microcosms; Sediment physicochemical properties (e.g., salinity, pH, total nitrogen, total phosphorus, and total organic carbon) across the studied lakes; Time-course variations of nitrate, nitrite, nitrous oxide, and Fe(II)/total Fe ratio in control enrichment cultures under NrAc, NrFe, and NrFeAc conditions; X-ray diffractograms (XRD) of precipitates from NrFe and NrFeAc enrichment cultures, with reference to halite background; Scanning electron microscopy (SEM) images coupled with energy-dispersive X-ray spectroscopy (EDS) analysis of mineral precipitates, highlighting iron detection and cell-mineral associations. Supplementary material to this article can be found online at https://doi.org/10.1016/j.gca.2026.03.028.

References

Bolyen, E., Rideout, J.R., Dillon, M.R., Bokulich, N.A., Abnet, C.C., Al-Ghalith, G.A., et al., 2019. Reproducible, interactive, scalable and extensible microbiome data science using QIIME 2. Nat. Biotechnol. 37, 852–857.

Buchwald, C., Grabb, K., Hansel, C.M., Wankel, S.D., 2016. Constraining the role of iron in environmental nitrogen transformations: dual stable isotope systematics of abiotic NO_2^- reduction by Fe(II) and its production of N_2O. Geochim. Cosmochim. Acta 186, 1–12.

Burgin, A.J., Hamilton, S.K., 2007. Have we overemphasized the role of denitrification in aquatic ecosystems? A review of nitrate removal pathways. Front. Ecol. Environ. 5, 89–96.

Emmerich, M., Bhansali, A., Lösekann-Behrens, T., Schröder, C., Kappler, A., Behrens, S., 2012. Abundance, distribution, and activity of Fe (II)-oxidizing and Fe (III)-reducing microorganisms in hypersaline sediments of Lake Kasin, southern Russia. Appl. Environ. Microbiol. 78, 4386–4399.

Gao, D., Gong, X., Su, H., Xu, A., Liu, Z., Liang, H., 2025. Impact of salinity stress on shifting microbial community and regulating N_2O and CO_2 dynamics in alkaline wetlands. J. Environ. Manage. 376, 124603.

Gao, Y., Zhang, G., Jiang, S., Liu, Y., 2024. Wekemo Bioincloud: a user-friendly platform for meta-omics data analyses. iMeta 3, e175.

Grimm, H., Lorenz, J., Straub, D., Joshi, P., Shuster, J., Zarfl, C., et al., 2024. Nitrous oxide is the main product during nitrate reduction by a novel lithoautotrophic iron (II)-oxidizing culture from an organic-rich paddy soil. Appl. Environ. Microbiol. 91, e01262-24.

Handley, K.M., Lloyd, J.R., 2013. Biogeochemical implications of the ubiquitous colonization of marine habitats and redox gradients by *Marinobacter* species. Front. Microbiol. 4, 136.

Hu, D., Zeng, Q., Liu, X., Hu, J., Guo, D., Dong, H., 2023. Ligand enhanced bio-oxidation of structural Fe (II) in illite coupled with nitrate reduction. Geochim. Cosmochim. Acta 357, 50–63.

Huang, J., Han, M., Yang, J., Kappler, A., Jiang, H., 2022. Salinity impact on composition and activity of nitrate-reducing Fe(II)-oxidizing microorganisms in saline lakes. Appl. Environ. Microbiol. 88 e00132-22.

Huang, J., Han, M., Yang, J., Wang, Y., Jiang, H., 2025a. Salinization influences the biodiversity-ecosystem functioning relationship more strongly at high salinity. mLife 4, 681–694.

Huang, J., Yang, J., Han, M., Wang, B., Sun, X., Jiang, H., 2023a. Microbial carbon fixation and its influencing factors in saline lake water. Sci. Total Environ. 877, 162922.

Huang, J., Mellage, A., Pavon-Garcia, J., Glöckler, D., Mahler, S., Elsner, M., et al., 2023b. Metabolic performance and fate of electrons during nitrate-reducing Fe(II) oxidation by the autotrophic enrichment culture KS grown at different initial Fe/N ratios. Appl. Environ. Microbiol. 89 e00196-23.

Huang, M., Li, J., Gan, Z., Huang, Y., Meng, F., 2025b. Efficient biological nitrate removal from hypersaline streams: denitrification performance and bacterial community succession. Water Res. 287, 124373.

Jakus, N., Blackwell, N., Osenbrück, K., Straub, D., Byrne, J.M., Wang, Z., et al., 2021. Nitrate removal by a novel lithoautotrophic nitrate-reducing iron (II)-oxidizing culture enriched from a pyrite-rich limestone aquifer. Appl. Environ. Microbiol. 87 e00460-21.

Jiang, H., Huang, J., Li, L., Huang, L., Manzoor, M., Yang, J., et al., 2021. Onshore soil microbes and endophytes respond differently to geochemical and mineralogical changes in the Aral Sea. Sci. Total Environ. 765, 142675.

Kappler, A., Schink, B., Newman, D.K., 2005. Fe(III) mineral formation and cell encrustation by the nitrate-dependent Fe(II)-oxidizer strain BoFeN1. Geobiology 3, 235–245.

Klueglein, N., Zeitvogel, F., Stierhof, Y.-D., Floetenmeyer, M., Konhauser Kurt, O., Kappler, A., Obst, M., 2014. Potential role of nitrite for abiotic Fe(II) oxidation and cell encrustation during nitrate reduction by denitrifying bacteria. Appl. Environ. Microbiol. 80, 1051–1061.

Lai, J., Zou, Y., Zhang, J., Peres-Neto, P.R., 2022. Generalizing hierarchical and variation partitioning in multiple regression and canonical analyses using the rdacca.hp R package. Methods Ecol. Evol. 13, 782–788.

Laufer, K., Røy, H., Jørgensen, B.B., Kappler, A., 2016. Evidence for the existence of autotrophic nitrate-reducing Fe (II)-oxidizing bacteria in marine coastal sediment. Appl. Environ. Microbiol. 82, 6120–6131.

Li, S., Wang, S., Pang, Y., Ji, G., 2022. Influence of electron donors (Fe, C, S) on N_2O production during nitrate reduction in lake sediments: evidence from isotopes and functional genes. ACS ES&T Water 2, 1254–1264.

Liu, C., Cui, Y., Li, X., Yao, M., 2021. microeco: an R package for data mining in microbial community ecology. FEMS Microbiol. Ecol. 97, fiaa255.

Liu, T., Chen, D., Li, X., Li, F., 2019. Microbially mediated coupling of nitrate reduction and Fe(II) oxidation under anoxic conditions. FEMS Microbiol. Ecol. 95, fiz030.

Melton, E.D., Swanner, E.D., Behrens, S., Schmidt, C., Kappler, A., 2014. The interplay of microbially mediated and abiotic reactions in the biogeochemical Fe cycle. Nat. Rev. Microbiol. 12, 797–808.

Messager, M.L., Lehner, B., Grill, G., Nedeva, I., Schmitt, O., 2016. Estimating the volume and age of water stored in global lakes using a geo-statistical approach. Nat. Commun. 7, 13603.

Miao, S., Jin, C., Liu, R., Bai, Y., Liu, H., Hu, C., Qu, J., 2020. Microbial community structures and functions of hypersaline heterotrophic denitrifying process: lab-scale and pilot-scale studies. Bioresour. Technol. 310, 123244.

Neal, C., Neal, M., Wickham, H., 2000. Phosphate measurement in natural waters: two examples of analytical problems associated with silica interference using phosphomolybdic acid methodologies. Sci. Total Environ. 251–252, 511–522.

Pan, D., Chen, P., Yang, G., Niu, R., Bai, Y., Cheng, K., et al., 2023a. Fe (II) oxidation shaped functional genes and bacteria involved in denitrification and dissimilatory nitrate reduction to ammonium from different paddy soils. Environ. Sci. Technol. 57, 21156–21167.

Pan, Y., She, D., Shi, Z., Cao, T., Xia, Y., Shan, J., 2023b. Salinity and high pH reduce denitrification rates by inhibiting denitrifying gene abundance in a saline-alkali soil. Sci. Rep. 13, 2155.

Pang, Y., Wang, J.-L., Li, S., Ji, G., 2021. Activity of autotrophic Fe(II)-oxidizing denitrifiers in freshwater lake sediments. ACS ES&T Water 1, 1566–1576.

Porsch, K., Kappler, A., 2011. Fe(II) oxidation by molecular O_2 during HCl extraction. Environ. Chem. 8, 190–197.
Qi, H., Liu, Y., 2023. Nitrogen removal through denitrification in China's aquatic system. Sci. Total Environ. 891, 164317.
Qin, Y., Yi, S., Ren, S., Li, N., Chen, J., 2014. Responses of typical grasslands in a semi-arid basin on the Qinghai-Tibetan Plateau to climate change and disturbances. Environ. Earth Sci. 71, 1421–1431.
Quast, C., Pruesse, E., Yilmaz, P., Gerken, J., Schweer, T., Yarza, P., et al., 2012. The SILVA ribosomal RNA gene database project: improved data processing and web-based tools. Nucleic Acids Res. 41, D590–D596.
Ravishankara, A., Daniel, J.S., Portmann, R.W., 2009. Nitrous oxide (N_2O): the dominant ozone-depleting substance emitted in the 21st century. Science 326, 123–125.
Seitzinger, S., Harrison, J.A., Böhlke, J., Bouwman, A., Lowrance, R., Peterson, B., et al., 2006. Denitrification across landscapes and waterscapes: a synthesis. Ecol. Appl. 16, 2064–2090.
Shu, D., He, Y., Yue, H., Yang, S., 2016. Effects of Fe (II) on microbial communities, nitrogen transformation pathways and iron cycling in the anammox process: kinetics, quantitative molecular mechanism and metagenomic analysis. RSC Adv. 6, 68005–68016.
Stookey, L.L., 1970. Ferrozine-a new spectrophotometric reagent for iron. Anal. Chem. 42, 779–781.
Su, J., Shao, S., Huang, T., Ma, F., Yang, S., Zhou, Z., Zheng, S., 2015. Anaerobic nitrate-dependent iron (II) oxidation by a novel autotrophic bacterium, *Pseudomonas* sp. SZF15. J. Environ. Chem. Eng. 3, 2187–2193.
Sun, X., Tan, E., Wang, B., Gan, Z., Yang, J., Han, J., et al., 2023. Salinity change induces distinct climate feedbacks of nitrogen removal in saline lakes. Water Res. 245, 120668.
Sun, X., Yang, J., Jiang, H., Wang, B., Xiao, H., Xie, Z., et al., 2022. Nitrite- and N_2O-reducing bacteria respond differently to ecological factors in saline lakes. FEMS Microbiol. Ecol. 98, fiac007.
Sun, X., Wang, B., Yang, J., Yu, H., Yao, B., Han, M., et al., 2025. Antagonistic effect of changing salinity and dissolved organic carbon on N_2O production via different pathways in saline lakes. Water Res. 285, 124111.
Thakur, I.S., Medhi, K., 2019. Nitrification and denitrification processes for mitigation of nitrous oxide from waste water treatment plants for biovalorization: challenges and opportunities. Bioresour. Technol. 282, 502–513.
Torregrosa-Crespo, J., Miralles-Robledillo, J.M., Bernabeu, E., Pire, C., Martínez-Espinosa, R.M., 2023. Denitrification in hypersaline and coastal environments. FEMS Microbiol. Lett. 370, fnad066.
Valiente, N., Gómez-Alday, J.J., Jirsa, F., 2019. Spectrophotometric determination of nitrate in hypersaline waters after optimization based on the Box-Behnken design. Microchem. J. 145, 951–958.
Valiente, N., Carrey, R., Otero, N., Soler, A., Sanz, D., Muñoz-Martín, A., et al., 2018. A multi-isotopic approach to investigate the influence of land use on nitrate removal in a highly saline lake-aquifer system. Sci. Total Environ. 631, 649–659.
Walters, W., Hyde, E.R., Berg-Lyons, D., Ackermann, G., Humphrey, G., Parada, A., et al., 2015. Improved bacterial 16S rRNA gene (V4 and V4–5) and fungal internal transcribed spacer marker gene primers for microbial community surveys. mSystems 1 e00009-15.
Wang, J., Zhang, H., Zhang, P., Xia, X., Liu, Y., Li, Y., Huo, S., 2025a. Salinity alters N_2O production pathway in lake sediments on the Qinghai–Tibet Plateau. J. Clean. Prod. 503, 145402.
Wang, M., Hu, R., Zhao, J., Kuzyakov, Y., Liu, S., 2016. Iron oxidation affects nitrous oxide emissions via donating electrons to denitrification in paddy soils. Geoderma 271, 173–180.
Wang, Z., Wan, Y., Ma, Z., Xu, L., Zhai, Y., Su, X., 2025b. Impact of iron minerals on nitrate reduction in the lake–groundwater interaction zone of high-salinity environment. Water 17, 1241.
Widdel, F., Bak, F., 1992. Gram-negative mesophilic sulfate-reducing bacteria. In: Balows, A., Trueper, H.G., Dworkin, M., Harder, W., Schleifer, K.H. (Eds.), The Prokaryotes. Springer, New York, pp. 3352–3378.
Williams, W.D., 1996. What future for saline lakes? Environ. 38, 12–39.
Willis, R.B., Montgomery, M.E., Allen, P.R., 1996. Improved method for manual, colorimetric determination of total Kjeldahl nitrogen using salicylate. J. Agric. Food Chem. 44, 1804–1807.
Wurtsbaugh, W.A., Miller, C., Null, S.E., DeRose, R.J., Wilcock, P., Hahnenberger, M., et al., 2017. Decline of the world's saline lakes. Nat. Geosci. 10, 816–821.
Xia, Y., Chen, X., Jiang, X., Shen, J., 2025. Enhanced denitrification under saline conditions: glycine betaine as a key osmoprotectant. Bioresour. Technol. 429, 132517.
Xue, C., Lin, H., Zhu, X., Liu, J., Zhang, Y., Rowley, G., et al., 2021. DiTing: a pipeline to infer and compare biogeochemical pathways from metagenomic and metatranscriptomic data. Front. Microbiol. 12, 698286.
Yang, J., Han, M., Zhao, Z., Jiang, H., 2022. Positive priming effects induced by allochthonous and autochthonous organic matter input in the lake sediments with different salinity. Geophys. Res. Lett. 49, e2021GL096133.
Yang, J., Jiang, H., Sun, X., Huang, J., Han, M., Wang, B., 2021. Distinct co-occurrence patterns of prokaryotic community between the waters and sediments in lakes with different salinity. FEMS Microbiol. Ecol. 97, fiaa234.
Zhang, L., Dong, H., Kukkadapu, R.K., Jin, Q., Kovarik, L., 2019. Electron transfer between sorbed Fe (II) and structural Fe (III) in smectites and its effect on nitrate-dependent iron oxidation by *Pseudogulbenkiania* sp. strain 2002. Geochim. Cosmochim. Acta 265, 132–147.
Zhang, S., Ali, A., Su, J., Huang, T., Li, M., 2022. Performance and enhancement mechanism of redox mediator for nitrate removal in immobilized bioreactor with preponderant microbes. Water Res. 209, 117899.
Zhao, L., Dong, H., Edelmann, R.E., Zeng, Q., Agrawal, A., 2017. Coupling of Fe (II) oxidation in illite with nitrate reduction and its role in clay mineral transformation. Geochim. Cosmochim. Acta 200, 353–366.
Zhao, L., Dong, H., Kukkadapu, R., Agrawal, A., Liu, D., Zhang, J., Edelmann, R.E., 2013a. Biological oxidation of Fe (II) in reduced nontronite coupled with nitrate reduction by *Pseudogulbenkiania* sp. strain 2002. Geochim. Cosmochim. Acta 119, 231–247.
Zhao, L., Dong, H., Kukkadapu, R.K., Zeng, Q., Edelmann, R.E., Pentrák, M., Agrawal, A., 2015. Biological redox cycling of iron in nontronite and its potential application in nitrate removal. Environ. Sci. Technol. 49, 5493–5501.
Zhao, W., Wang, Y., Liu, S., Pan, M., Yang, J., Chen, S., 2013b. Denitrification activities and N_2O production under salt stress with varying COD/N ratios and terminal electron acceptors. Chem. Eng. J. 215–216, 252–260.
Zumft, W.G., Körner, H., 1997. Enzyme diversity and mosaic gene organization in denitrification. Antonie Van Leeuwenhoek 71, 43–58.